Thermochimica Acta, 14 (1976) 25–40

AMORPHOUS TO CRYSTALLINE TRANSFORMATION IN BULK ELECTROLESS NICKEL BY DIFFERENTIAL SCANNING CALORIMETRY*

M. S. GREWAL, S. A. SASTRI AND B. H. ALEXANDER
Boston Research and Development Laboratory, The Gillette Company, South Boston, Mass. 02106 (U.S.A.)

ABSTRACT

Differential scanning calorimetry (DSC) in conjunction with X-rays and transmission electron microscopy were employed to elucidate the mechanism of amorphous to crystalline transformation in bulk electroless nickel (Ni—10.9 wt. % P) alloy. As-deposited amorphous electroless nickel was heated from room temperature to 650°C in a DSC cell in an argon atmosphere at 20°C min^{-1}. Three exothermic reactions were observed. Heating runs were interrupted after each reaction for microstructural and crystal structure determinations. It was found that the first reaction was associated with the precipitation of fine nickel particles in an amorphous Ni_3P matrix, the second with crystallization of the amorphous Ni_3P matrix into spherulitic grains, and the third with recrystallization and grain growth of the Ni_3P matrix and coarsening of nickel precipitates. The transformation temperatures and heats of reaction were also determined. This demonstrates the application of high sensitivity differential scanning calorimetry to the study of solid state reactions in general.

INTRODUCTION

When a metal or alloy is quenched or cooled at a very fast rate from the liquid state, an amorphous or non-crystalline structure is formed. In other words, one can preserve the liquid state structure in a solid by a high rate of cooling. Such a structure is characterized by having a short range order or clustering of atoms, and the absence of any long range order such as is found in crystalline solids. The above method of producing non-crystalline solids is called splat cooling[1].

Amorphous structures can also be obtained by vapor quenching[2] on a cold substrate, by chemical deposition from solution (electroless deposition)[3] or by electrodeposition from solution[4]. Numerous applications have been developed for electroless nickel deposits and electroless nickel has been the subject of several investigations[5–16].

*Presented at the 5th North American Thermal Society Meeting, Peterborough, Ontario, Canada, June 8–14, 1975.

Most of the literature on electroless nickel deals with the details of the process, i.e., the chemistry of deposition[5]. Some work has also been reported on the structural aspects[6–8,12–14] of as-deposited alloy and aspects of physical[8–11] and mechanical properties[7]. Even there, discrepancies exist about the effects of heat treatment on the physical and mechanical properties of electroless nickel deposits.

The structure of as-deposited electroless nickel thin films is well established to be amorphous or liquid-like[9,12–14]. The structure of bulk electroless nickel, however, was reported to be either amorphous[6] or finely polycrystalline[7].

Randon et al.[15] carried out DTA and X-ray studies of electroless nickel and mixture of nickel and phosphorous powders. DTA analysis of electroless nickel (4–12 wt. % P) showed a diffused low intensity peak covering 200–300°C and a sharp peak at 310°C.

Schlesinger and Marton[10] observed, upon heating the as deposited Ni–P films in vacuum, the crystallization taking place at a characteristic temperature of 350°C. Bagley and Turnbull[12] recently studied the transformation of thin films of amorphous electro-deposited Ni–P alloy (Ni—14.9 wt. % P) using differential scanning calorimetry (DSC). They observed two exothermic transformations, the first of which occurred at 280°C and the second at 410°C.

The current authors have recently made a detailed study on the mechanism of the amorphous to crystalline transformation in bulk electroless nickel using various techniques as follows: differential thermal analysis (DTA), differential scanning calorimetry (DSC), thermal mechanical analysis (TMA), X-ray and electron diffraction methods, optical scanning and transmission electron microscopy, and microhardness measurements.

This paper deals with the use of thermal analysis, especially DSC, to study the mechanism of amorphous to crystalline transformation in electroless nickel. This detailed study would not have been possible without the use of DSC. This study demonstrates the application of high sensitivity differential scanning calorimetry to the study of solid state reactions in general.

EXPERIMENTAL

The bulk electroless nickel used in this investigation had been deposited on a nickel cathode to a thickness of 0.17 inches, and on a cast iron wheel to a thickness of 0.02" from a standard production plating bath[17]. The chemical analysis of the deposit showed an average composition of 10.9 wt. % P, balance Ni, which is very close to the eutectic composition[18] (see Fig. 1). Spectrographic analysis revealed traces of Fe, Si, Mn, and Cu. Heat treatments were carried out in a tube furnace with a hydrogen atmosphere. A DuPont 990 Thermal Analyzer was used to perform DSC, DTA and TMA analysis. DSC runs were interrupted at various stages of the transformation for hardness measurements, microstructural observations, and X-ray diffraction analysis. Hardness measurements were made on the well-prepared metallographic samples with either a Leitz or a Zeiss microhardness tester. Samples for transmission

electron microscopy were prepared with an automatic dual-jet polisher using a specially prepared electrolyte, and operating it at optimum conditions[19]. They were examined with one of two electron microscopes, namely a Philips (100 Kv) and a Hitachi (200 Kv). X-ray diffraction analyses were done using a Siemens X-ray diffraction unit with Cu–K_α radiation.

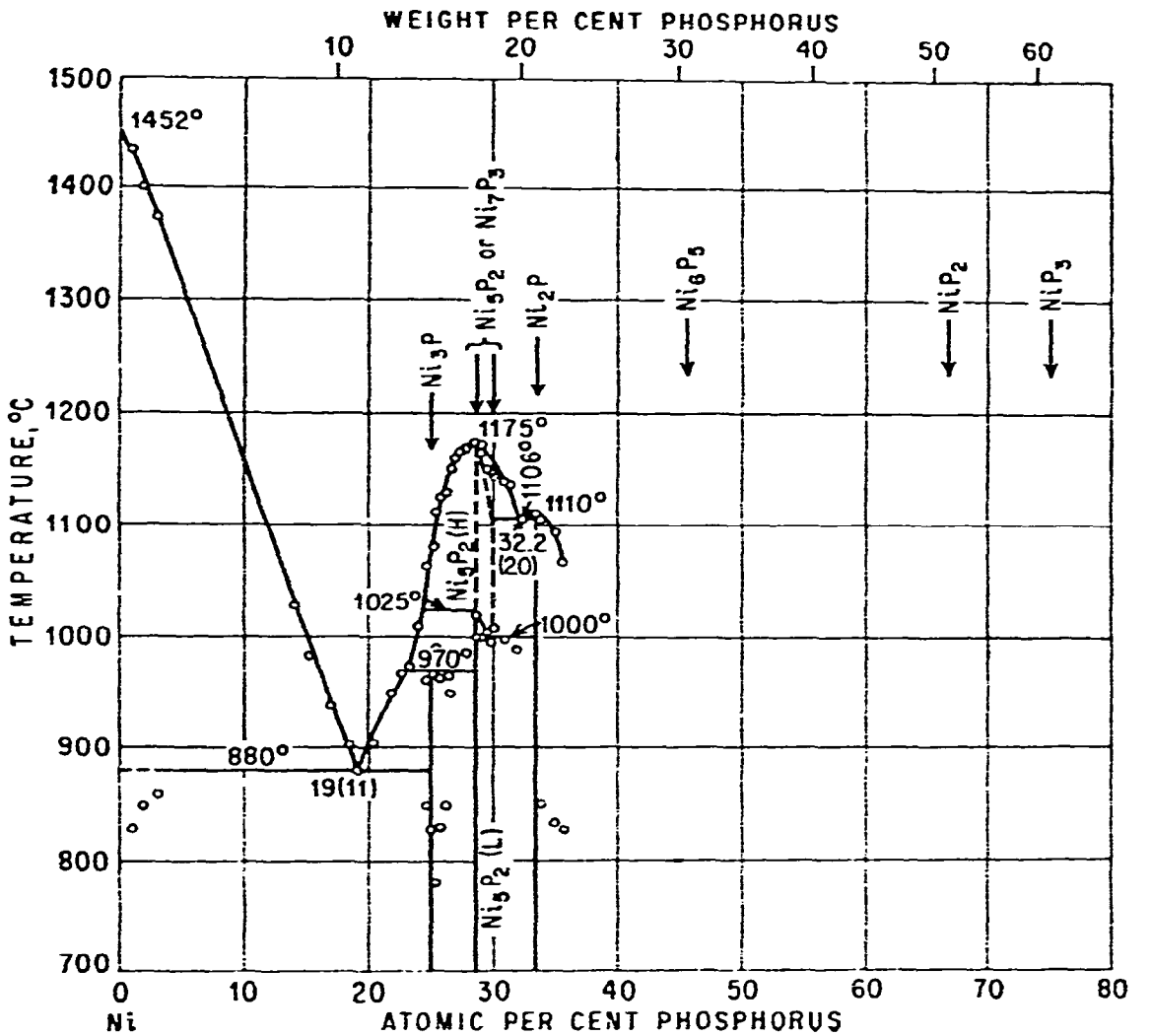

Fig. 1. Ni–P phase diagram.

RESULTS AND DISCUSSION

(1) *Nature of electroless nickel deposits*

As-deposited electroless nickel showed a lamellated structure, the lamellae parallel to the base metal (Fig. 2). These bands are believed to have resulted from the periodic variations in the phosphorous content of the deposit. Chemical analysis

of the deposit showed phosphorous variation between 9 and 11 wt. % with an average phosphorous content of 10.9 wt. %. This is close to the eutectic composition in the Ni–P binary alloy. The equilibrium phase diagram[18] for Ni–P is shown in Fig. 1, which shows a low melting eutectic (880 °C; 1616 °F) at 11 wt. % phosphorous.

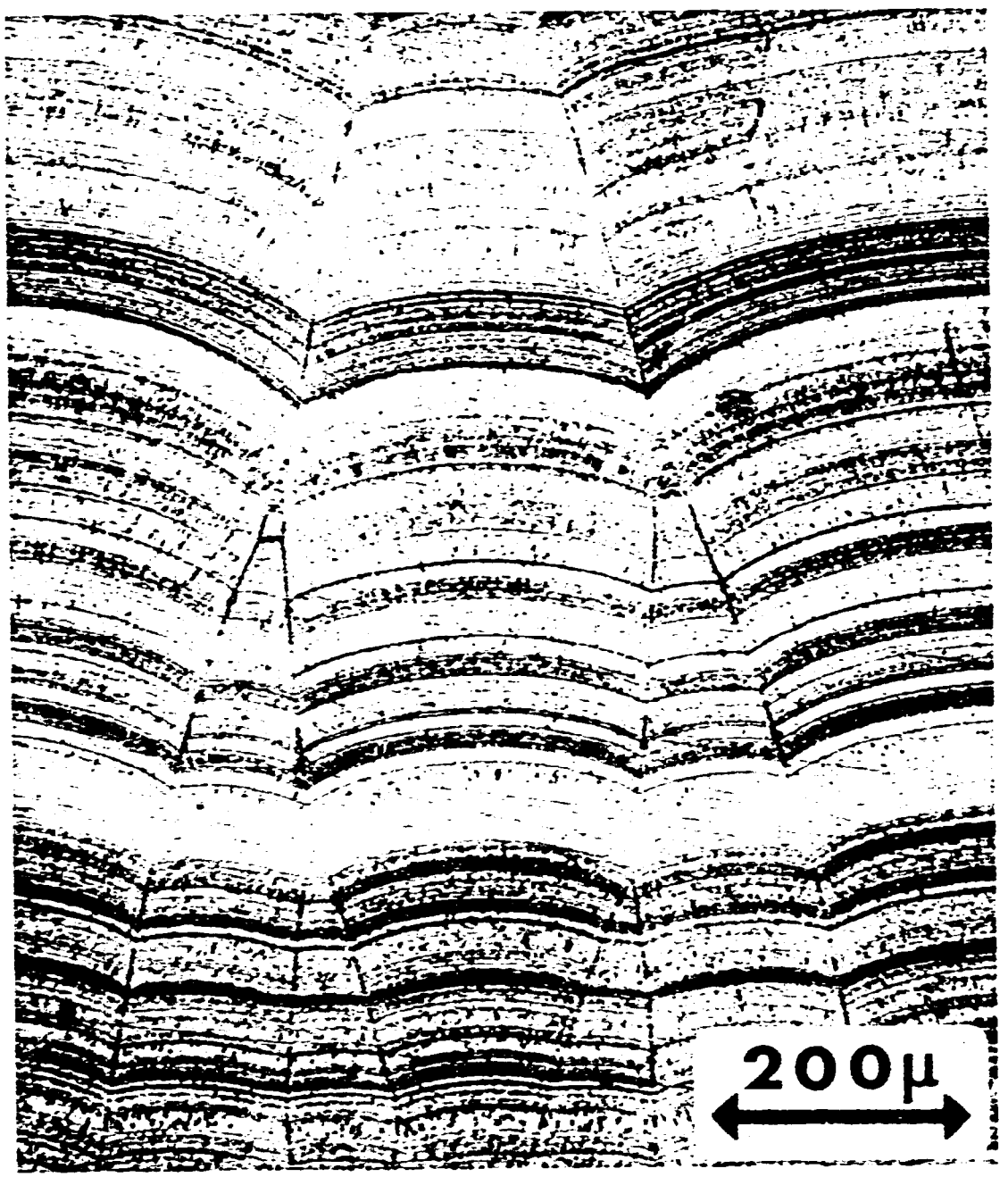

Fig. 2. Electroless nickel as deposited. Etched electrolytically in 5% H_2SO_4.

The melting point of our alloy was found to be 910°C. The microstructure of a sample slowly cooled from the melt showed a eutectic structure (Fig. 3). This confirms the results of the chemical analysis.

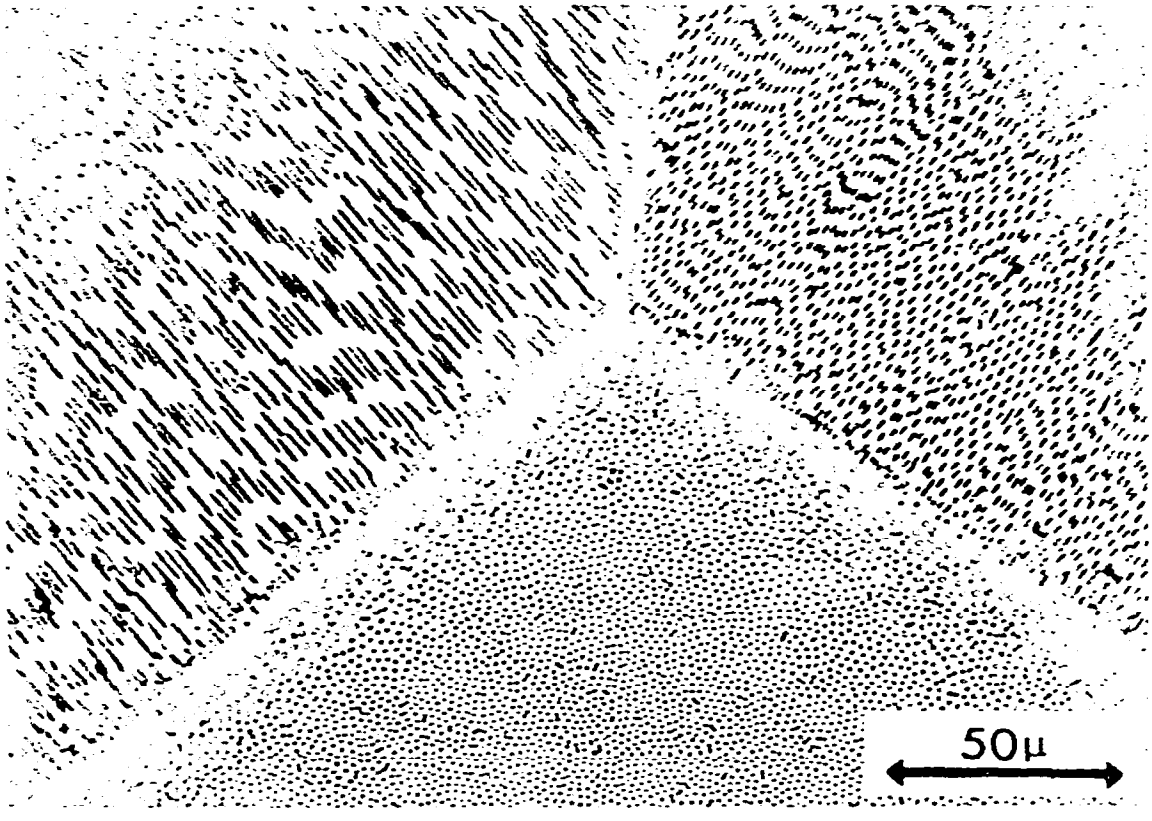

Fig. 3. Optical micrograph of electroless nickel cooled from melt showing eutectic structure. Etchant: Carapella's reagent.

Figure 4 is a transmission electron micrograph and selected area diffraction (SAD) pattern of the as-deposited sample. The broad diffused ring in the SAD pattern is indicative of a lack of long range crystallinity. This type of diffraction pattern is typical of amorphous or liquid metal structures[14]. X-ray diffraction also confirms this finding. The average hardness of the as-deposited sample was 600 DPHN.

(2) *Effects of heat treatment*

The effect of heat treatment on the hardness was studied at temperatures from 200 to 1600°F with various holding times[20]. The results of the time–temperature effect on the hardness are shown in Table 1 and Figs. 5 and 6. A hardness of about 1100 DPHN is reached by heating the alloy for a few minutes between 700 and 800°F. It takes about one hour to reach the same hardness when the alloy is heated at 600°F. This shows that the hardening is associated with some kind of time–temperature

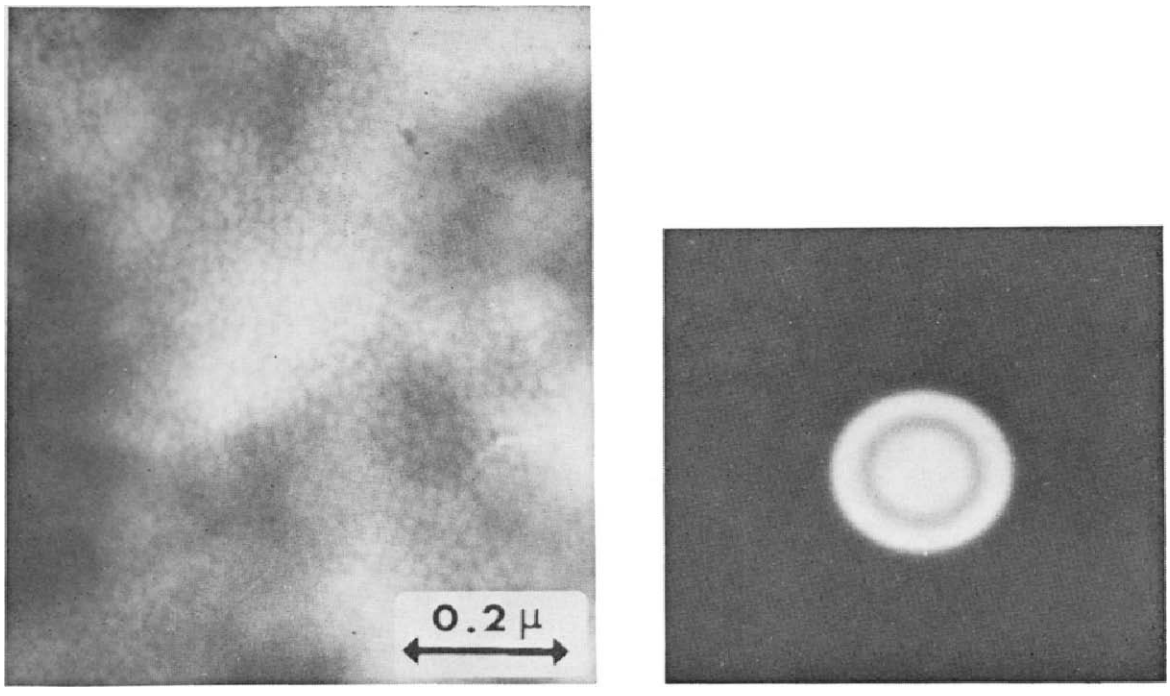

Fig. 4. Transmission electron micrograph and SAD pattern of as deposited amorphous electroless nickel.

dependent reaction or transformation. X-ray analysis of the fully hardened samples shows the presence of crystalline nickel and Ni_3P. The hardening upon heat treatment of amorphous nickel seems to be associated with the amorphous to crystalline transformation.

(3) *Mechanism of amorphous to crystalline transformation*

To study the mechanism of amorphous to crystalline transformation, we employed DTA, DSC and TMA in conjunction with electron microscopy and X-ray diffraction. The results of these studies are presented below:

(A) *Differential thermal analysis (DTA).* A DuPont 1600°C cell was used as a module in the DuPont 990 thermal analyzer. Samples were heated at 20°C min^{-1} in an argon atmosphere. High purity alumina was used as a reference material. A typical DTA scan is presented in Fig. 7. The first peak (exotherm) is associated with crystallization of electroless nickel and the second peak (endotherm) is associated with the melting of the alloy.

(B) *Differential scanning calorimetry (DSC).* The DuPont DSC cell module was used with the DuPont 990 thermal analyzer. Samples weighing 70–80 mg were heated between room temperature and 650°C in an argon atmosphere at 20°C min^{-1}. Figure 8 shows a typical DSC trace. The three exothermic peaks observed are labeled as Stage I, II and III. Both the transformation temperatures (at onset of transformation) and transformation energies were determined from the DSC scan. A calibration

TABLE 1

EFFECT OF HEATING TIME AND TEMPERATURE ON THE HARDNESS OF ELECTROLESS NICKEL (Ni—10.8 wt. % P) ALLOY
As cast from 1850°—600 DPHN.

Temp. (°F)	*Microhardness, DPHN*[a]							
	Heating Time							
	Minutes			*Hours*				
	2	*10*	*30*	*2*	*4*	*8*	*16*	*32*
200	—	—	623	—	—	—	—	—
300	—	—	630	—	—	—	—	—
400	—	—	645	—	—	—	—	—
500	626	683	703	706	—	728	822	—
600	682	900	1088	1130	1132	1135	—	—
700	1100	1132	1145	1140	1130	1135	1130	1132
800	1115	1142	1145	1140	1137	1135	1132	1135
900	—	—	1056	—	—	—	—	—
1000	—	1042	971	—	956	—	—	—
1100	—	—	853	—	—	—	—	—
1200	—	938	795	—	785	—	—	—
1300	—	—	726	—	—	—	—	—
1400	—	—	712	—	—	—	—	—
1500	—	762	650	—	635	—	—	—
1600	—	—	592	—	—	—	—	—

[a] Diamond Pyramid Hardness as determined using a Leitz microhardness tester, 100g load. Reported values are averages of 5 to 10 measurements.

of the DSC cell using the heats of fusion of indium, tin, lead, and zinc standards was carried out. The details of the method used to determine the transformation energies are described elsewhere[21,22]. The onset of the first stage of transformation occurred at 150 ±2°C (T_I), with an energy of 0.5 cal g^{-1}, the second at 335 ±5°C (T_{II}), with an energy of 24.0 cal g^{-1} and the third at 400 ±5°C (T_{III}) with an energy of 1.5 cal g^{-1}. The DSC runs were interrupted at 250, 310, 375 and 500°C to determine hardness, crystal structure and microstructure. These results are presented below.

The microstructure and SAD pattern of the sample run in DSC from room temperature to 250°C are shown in Fig. 9. Note the very fine nickel precipitates (black dots) appearing in an otherwise amorphous matrix. Tilting the specimen in the electron microscope showed these precipitates to be very thin plates. These thin platelets lie in the plane perpendicular to the direction of the electroless nickel deposit. The broad diffused rings in the SAD pattern in Fig. 9 are from the amorphous matrix, and the faint spotty rings are the result of the crystalline nickel platelets precipitating out. X-ray diffraction analysis showed slight sharpening of the diffused broad peak at d ~2.03 Å and appearance of the two other weak broadened lines at 1.24 and 1.06 Å. This also shows the precipitation of crystalline nickel of small

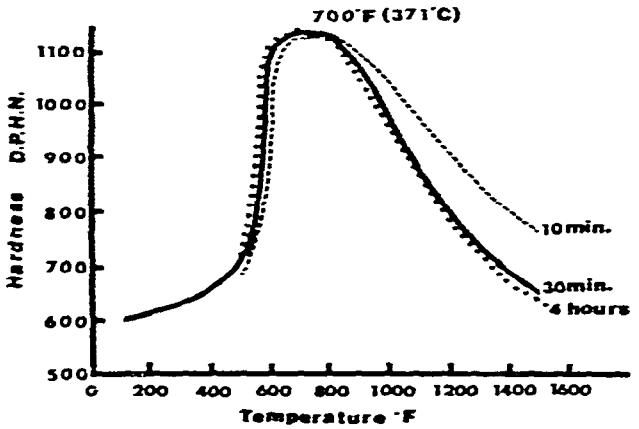

Fig. 5. Effect of temperature and heating time on hardness of bulk electroless nickel deposits.

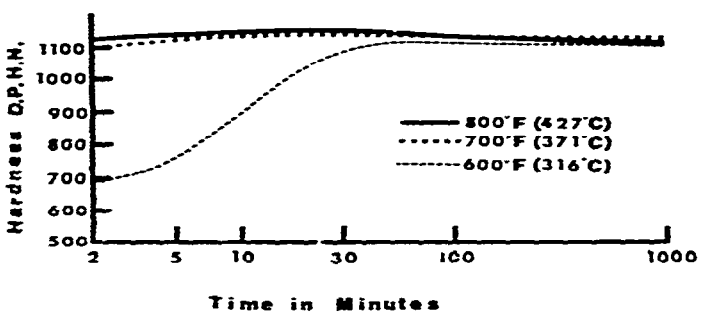

Fig. 6. Effect of temperature and heating time on hardness of bulk electroless nickel deposits.

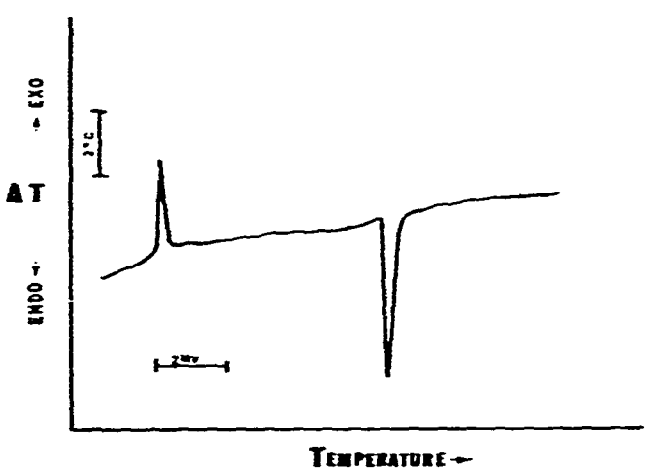

Fig. 7. DTA trace of electroless nickel. Heating rate 20 °C min^{-1}.

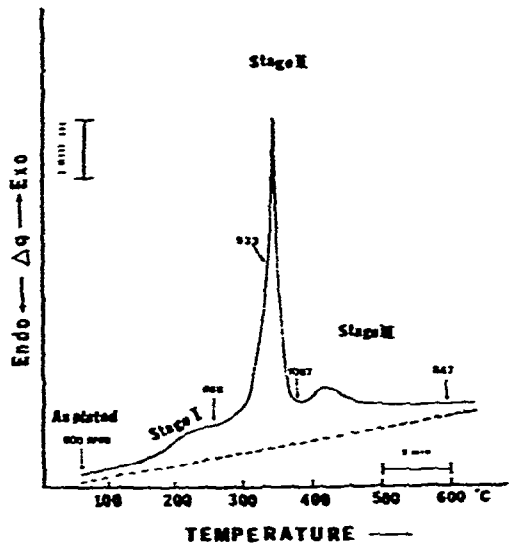

Fig. 8. DSC scan of electroless nickel showing various stages of transformation with corresponding hardness values.

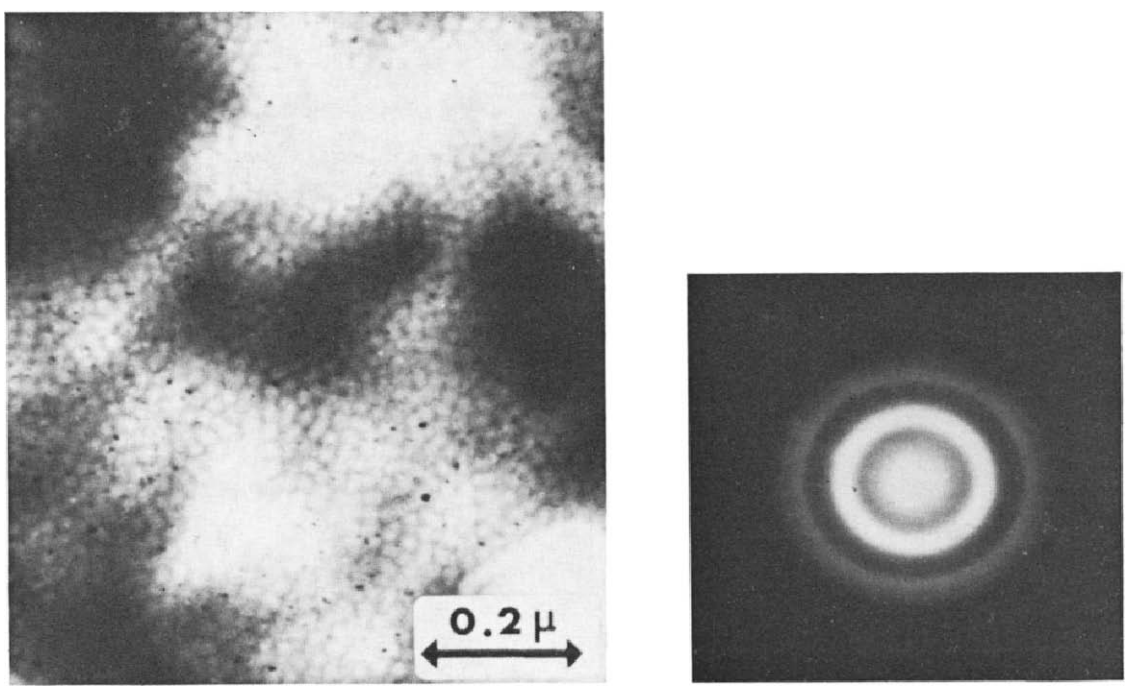

Fig. 9. Transmission electron micrograph and SAD pattern of electroless nickel heated to 250 °C showing fine nickel precipitates in the amorphous Ni_3P matrix.

crystallite size. The hardness of the sample at this stage was about 665 DPHN, which is not appreciably different from that of the as-deposited sample (600 DPHN).

A heating run interrupted at 310 °C and cooled to room temperature produced the microstructure shown in Fig. 10. The hardness value at this stage was 993 DPHN. Here the transformation of amorphous matrix to crystalline Ni_3P is shown to have

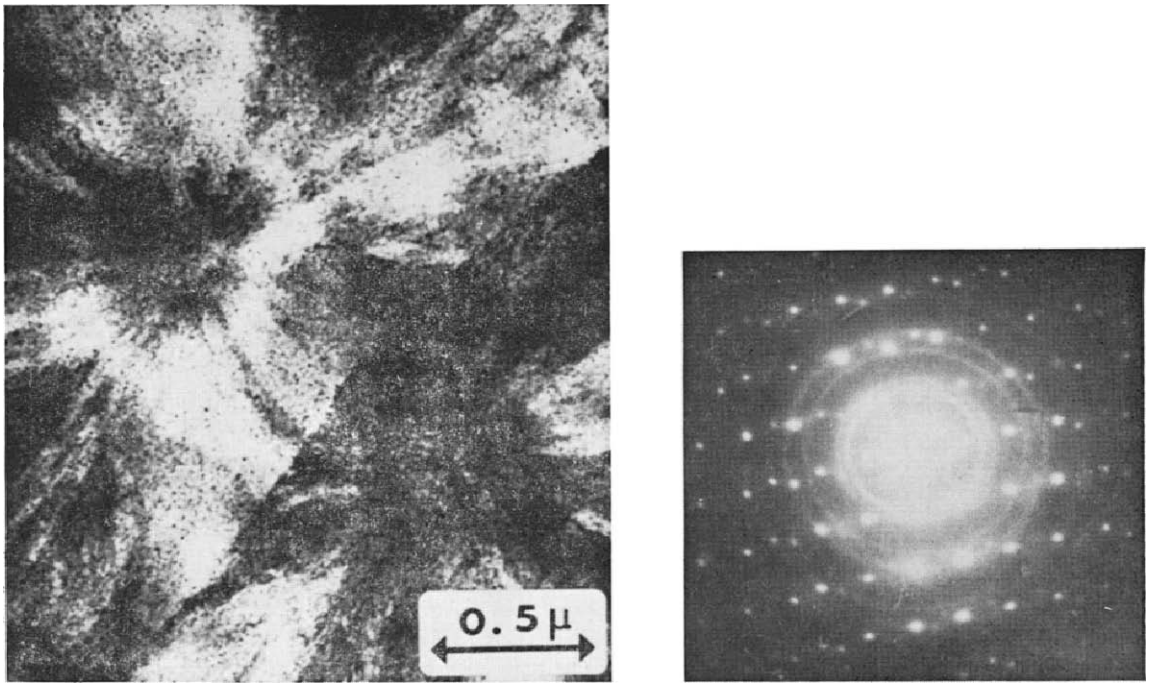

Fig. 10. Transmission electron micrograph and SAD pattern of electroless nickel heated to 310 °C showing the early stage of crystallization of the Ni_3P matrix into spherulitic grains.

proceeded with the formation of spherulites. The micrograph also shows fine dispersion of nickel crystallites in the now crystalline Ni_3P matrix. This is inferred from the SAD pattern, in which the continuous fine rings originate from the fine nickel particles, and the spot pattern is from the relatively large spherulitic Ni_3P grains. The Ni_3P spherulites seem to grow radially from the center. Note the boundary between two spherulites which resulted from impingement of one growing spherulite with another, shown in Fig. 10. This kind of spherulitic morphology is generally observed in polymers cooled from the melt or metals solidified from the liquid state[16]. Similar morphology was also reported in vapor deposited amorphous Ni–P film prepared by a flash evaporation technique[14].

The amorphous to crystalline transformation in our sample was found to be complete at 375 °C as shown in Fig. 11. Note some coarsening of the nickel dispersoid in the micrograph, and note also the multiple diffraction effect in the SAD pattern. Here again the spot pattern corresponds to the crystalline nickel. X-ray diffraction analysis of the sample at this stage also showed the presence of crystalline nickel and

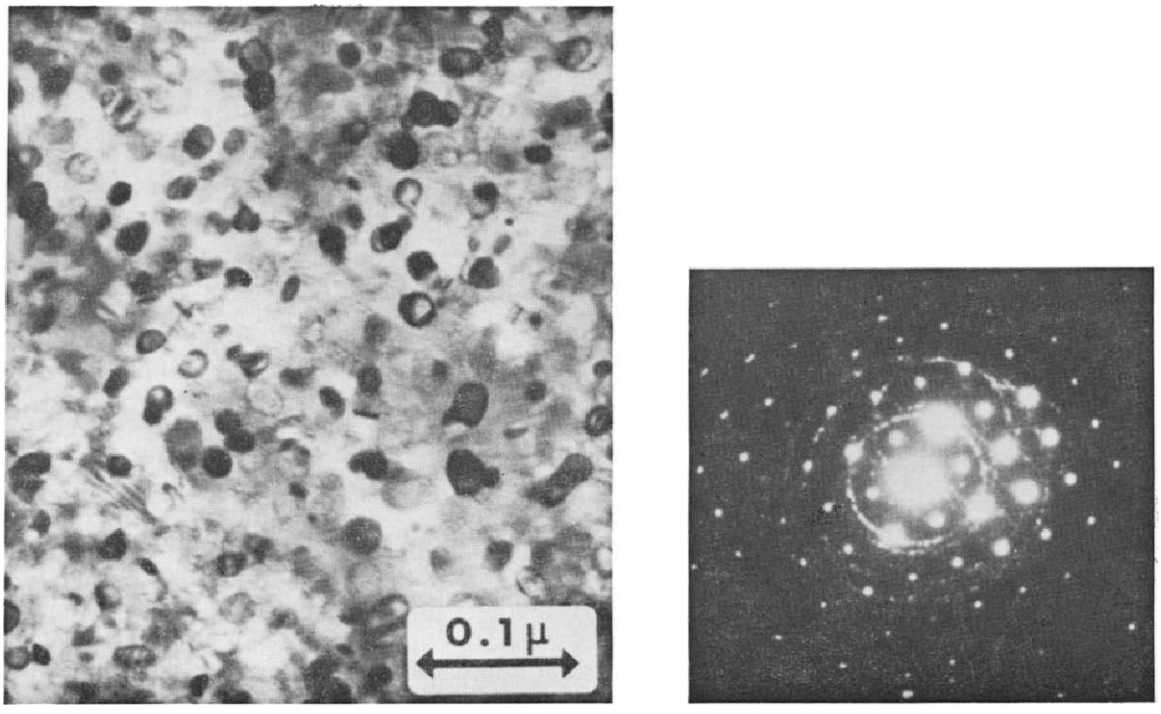

Fig. 11. Transmission electron micrograph and SAD pattern of electroless nickel sample heated to 375 °C showing completion of crystallization of the Ni_3P matrix.

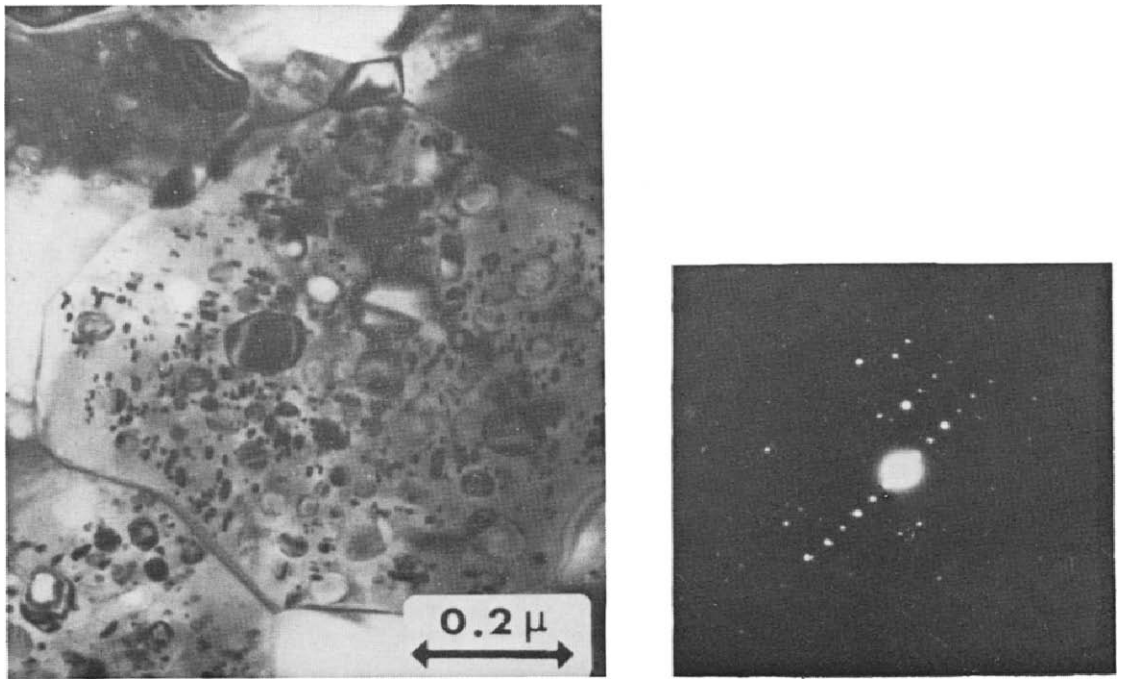

Fig. 12. Transmission electron micrograph and SAD pattern of electroless nickel sample heated to 500 °C showing recrystallization, grain growth of the Ni_3P matrix and coarsening of Ni precipitates.

Ni_3P. The completion of amorphous to crystalline transformation at this stage seems to correspond to the maximum hardness of about 1100 DPHN obtainable in this alloy.

Heating the as-deposited sample to 500°C gave rise to recrystallization of the Ni_3P matrix and coarsening of the Ni particles as shown in Fig. 12. This results in a drop in the hardness value from 1100 DPHN to 845 DPHN. Note that the spherulitic morphology has now been replaced by normal grain boundaries, and the structure looks like any other recrystallized material.

The high hardness value of the electroless nickel as a result of heating to 375°C from the amorphous state is caused by a microstructure consisting of a fine dispersion of Ni particles in a crystalline Ni_3P matrix. This is consistent with the accepted theory of precipitation hardening, which requires a crystalline lattice as the matrix. Most of the investigators[5,6,23] report that the final microstructure of electroless nickel after heat treatments consists of a fine dispersion of Ni_3P in a nickel matrix. Our study indicates that the reverse is true, in agreement with Ziehlke et al.[24]. This discrepancy, we believe, could be due to the difference in phosphorous content of electroless nickel alloys studied, i.e., depending on whether the alloy composition was hyper-eutectic or hypo-eutectic.

TABLE 2

EFFECT OF ISOTHERMAL ANNEALING AT 300 C ON TRANSITION TEMPERATURES

Time (min)	*Temp.* (°C)		
	T_I	T_{II}	T_{III}
15	—	335	400
30	—	330	395
60	—	310	390
180	—	—	385

TABLE 3

EFFECT OF HEATING RATE ON TRANSITION TEMPERATURES

Heating rate (°C min^{-1})	*Temp.* (°C)		
	T_I	T_{II}	T_{III}
5	—	315	—
10	145	325	390
20	150	335	400
50	175	350	410
100	225	360	425

The effect of isothermal annealing at 300°C for various lengths of time on the transition or transformation temperature is shown in Table 2. The higher the holding time during isothermal annealing, the lower is the transition temperature. Note that the crystallization peak disappears in specimens annealed 3 h at 300°C.

The effect of varying the heating rate from 5°C min^{-1} to 100°C min^{-1} on the transformation temperatures was also investigated. The results of this are presented in Table 3. At a very slow rate of heating (5°C min^{-1}) we observed just one broad crystallization peak at 315°C; increasing the rate of heating to 10°C min^{-1} or

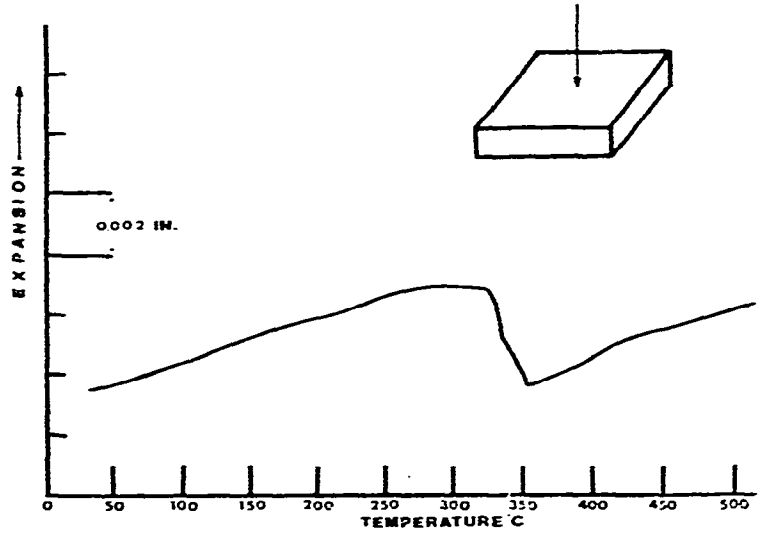

Fig. 13. TMA trace of electroless nickel in the direction of deposition. Heating rate 10 C min^{-1}.

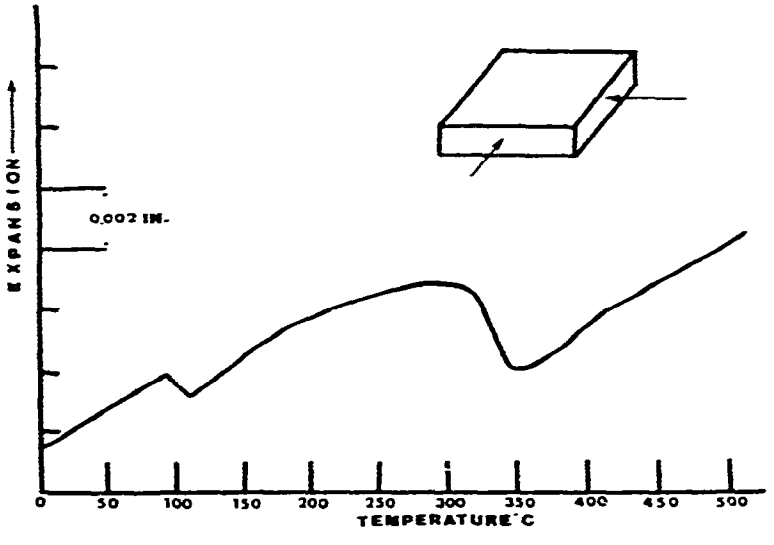

Fig. 14. TMA trace of electroless nickel along the plane of deposition. Heating rate 10°C min^{-1}.

higher resolved the three stages of transformation. Further, increasing the heating rate increased the observed transition temperatures. These observations confirm the earlier findings that the amorphous to crystalline transformation in electroless nickel (Ni—10.9 wt. % P) alloy is a time–temperature dependent reaction.

(C) *Thermomechanical analysis (TMA)*. A DuPont 942 thermomechanical analyzer was used in conjunction with the DuPont 990 thermal analysis system to obtain the phase transition or transformation temperature. Rectangular specimens, $0.25 \times 0.25 \times 0.120$ in., with the 0.120 in. dimension parallel to the direction of deposition, were prepared by wet milling. The specimen was kept at room temperature during this operation. TMA runs were made in an argon atmosphere both parallel to and normal to the direction of deposition, at a heating rate of $10\,^{\circ}C\ min^{-1}$.

The TMA trace in the direction of deposition is shown in Fig. 13. The contraction between 310 and 350 °C is due to the crystallization of amorphous Ni_3P, and this trace substantiates the earlier DSC findings.

Figure 14 shows the TMA trace in the direction normal to the direction of deposition, i.e., along the plane of deposition. Two transitions are to be noted here. The first one, at about 100 °C we believe to be associated with the precipitation of crystalline nickel platelets in the amorphous Ni_3P matrix. This will correspond to the first stage of transformation in the DSC scan (Fig. 8). This transition is not observed in the direction of deposition (Fig. 13). Transmission electron microscopy shows the precipitation of crystalline nickel as thin platelets in the plane of deposition, i.e., normal to the direction of deposition. The difference in the onset of the transformation may be due to the difference in heating rates. It is also probable that this transition may be associated with some intermediate phase formation before crystalline nickel precipitates out. However, this is highly unlikely because X-ray diffraction analysis did not show the presence of any other phase. The second transition is the same as observed in Fig. 13, namely the transition due to the crystallization of Ni_3P.

CONCLUSIONS

Differential scanning calorimetric (DSC) studies performed on electroless nickel (Ni—10.9 wt. % P) alloy showed the amorphous to crystalline transformation to take place in three distinct stages. Microstructure and selected area diffraction (SAD) patterns corresponding to the critical stages of the transformation are shown on the DSC scan (Fig. 15). As-deposited electroless nickel has an amorphous or liquid-like structure. The onset of the first stage of the transformation occurred at 150 $\pm 2\,^{\circ}C$ with an energy of 0.5 cal g^{-1}. This was found to be associated with precipitation of crystalline nickel in an amorphous Ni_3P matrix. The crystallization of Ni_3P occurred during the second stage of the transformation at 335 $\pm 5\,^{\circ}C$ with an energy of 24.0 cal g^{-1}. The third stage of the transformation occurred at 400 $\pm 5\,^{\circ}C$ with an energy of 1.5 cal g^{-1}. During this stage, recrystallization and grain growth of the Ni_3P matrix occurred. Some coarsening of the nickel precipitates was also observed.

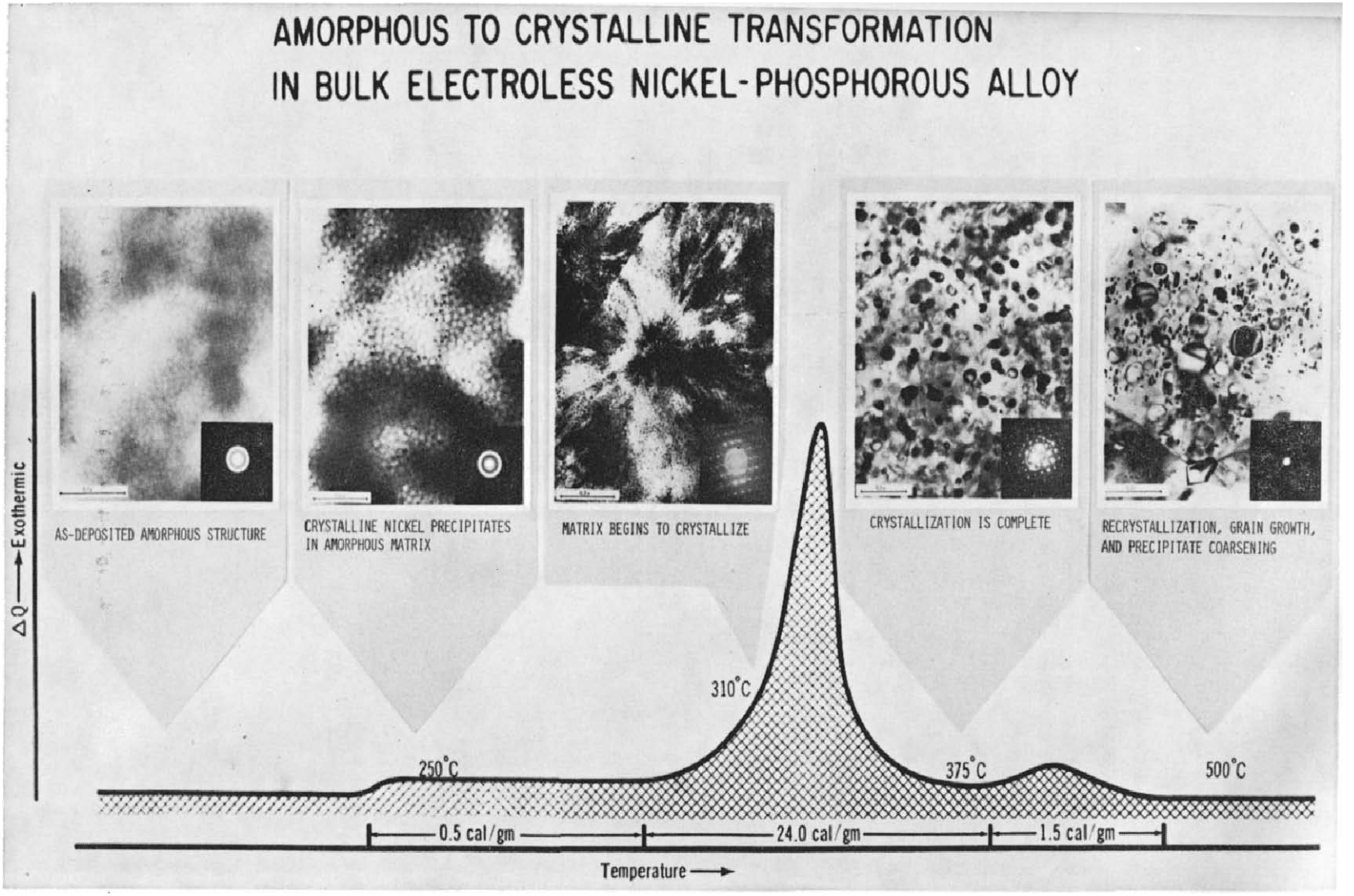

Fig. 15. Microstructures and SAD patterns corresponding to the critical stages of transformation on schematic DSC scan.

The technique described in this paper for studying the amorphous to crystalline transformation is quite general and can be applied to the study of other solid state reactions.

ACKNOWLEDGEMENTS

The authors are grateful to S. Hahn, A. Carefoot and L. Griffin for assistance in the experimental work, and F. Willett, M. Reavey and A. Hogan in preparing this manuscript.

REFERENCES

1 P. Duwez and R. H. Willens, *Trans. Met. Soc. AIME*, 227 (1965) 362.
2 S. Mader, *J. Vac. Sci. Technol.*, 2 (1965) 35.
3 A. Brenner and G. Riddell, Research Paper No. 1835, *J. Res. Nat. Bur. Stand.*, 39 (1947) 385; *Proc. Am. Electroplaters Soc.*, 34 (1947) 156.
4 A. Brenner, D. E. Couch and E. K. Williams, *J. Res. Nat. Bur. Stand.*, 44 (1950) 109; *Plating*, 37 (1950) 36.
5 *Chemical Reactions—Symposium on Electroless Nickel Plating*. ASTM Special Technical Publication No. 265 (1959).
6 A. W. Goldenstein, W. Rostaker, F. Schossborger and G. Gutzeit, *J. Electrochem. Soc.*, 104 (1957) 104.
7 A. H. Graham, R. W. Lindsay and H. J. Read, *J. Electrochem. Soc.*, 112 (1965) 401.
8 J. P. Marton and M. Schlesinger, *Bull. Am. Phys. Soc.*, 12 (1967) 394.
9 J. P. Marton and M. Schlesinger, *J. Electrochem. Soc.*, 115 (1968) 16.
10 M. Schlesinger and J. P. Marton, *J. Phys. Chem. Solids*, 20 (1968) 188.
11 M. Schlesinger and J. P. Marton, *J. Appl. Phys.*, 40 (1969) 507.
12 B. G. Bagley and D. Turnbull, *J. Appl. Phys.*, 39 (1968) 5681.
13 G. S. Cargil, III, *J. Appl. Phys.*, 41 (1970) 12.
14 B. G. Bagley and D. Turnbull, *Acta Met.*, 18 (1970) 857.
15 J. P. Randin, P. A. Maire, E. Saurer and H. E. Hintermann, *J. Electrochem. Soc.*, 114 (1967) 465.
16 M. S. Grewal, S. A. Sastri and B. H. Alexander, *Microstruct. Sci.*, 2 (1974) 147.
17 R. W. F. Morel, Paper Mate Manufacturing Company, Report No. 153 (1962).
18 P. M. Hansen, *Constitution of Binary Alloys*, McGraw-Hill, New York, 2nd ed., 1958, p. 1027.
19 S. A. Sastri and A. F. Carefoot, *Gilette R & D Technical Note*, No. 218 (1972) 4.
20 A. E. Jansson, L. R. McNall and A. Resta, *Paper Mate Manufacturing Company, Research Report*, No. 165 (1963) 4.
21 R. A. Baxter, *Thermal Analysis*, Academic Press, New York, 1969, p. 65.
22 G. W. Miller and J. L. Wood, *J. Therm. Anal.*, 2 (1970) 71.
23 W. G. Lee, *Plating*, 47 (1960) 288.
24 K. T. Ziehlke, W. S. Dritt and C. H. Mahoney, *Metal Progr.*, 77 (1960) 84.